doi:10.14311/ppt.2025.3.197
Plasma Physics and Technology **12**(3):197–201, 2025

CHARACTERIZING THE DIFFUSE VACUUM ARC VOLTAGE FOR MVDC CIRCUIT BREAKER APPLICATIONS: EXPERIMENT, DATA, AND EMPIRICAL MODEL

P. Wienkamp*, W. Leterme

IAEW at RWTH Aachen University, Schinkelstrasse 2, 52062 Aachen, Germany

* p.wienkamp@iaew.rwth-aachen.de

Abstract. Proposed hybrid DC circuit breaker concepts rely on the arc voltage in vacuum interrupters to commutate fault currents to parallel branches. This paper presents an extensive experimental investigation of the diffuse vacuum arc voltage of an industrially manufactured vacuum interrupter which is connected to a Thomson coil actuator. By independently varying the opening speed and arc current, an empirical model describing the diffuse vacuum arc voltage as a function of contact distance and current is derived. The model limits are evaluated by discussing the transition phase towards high-current anode mode formation.

Keywords: actuator, arc voltage, diffuse vacuum arc, vacuum interrupter.

1. Introduction

The increasing power infeed of distributed energy resources to the medium voltage (MV) power grid introduces new challenges to the existing infrastructure. Consequently, medium voltage direct current (MVDC) systems are being considered as a means to reduce system losses and increase operational flexibility [1]. However, in DC systems, fault currents are characterized by a fast increase, high steady-state value and absence of zero crossings. Therefore, new technologies to clear fault currents and isolate faulted equipment are required, to enable safe and reliable operation [2].

The natural arc commutation hybrid DC circuit breaker (HDCCB) is a promising and cost-effective solution for the lower end of the MV level. It was first proposed in [3] and a 4 kA/3 kV prototype was developed. This concept features a mechanical switch for the low-loss nominal operation, which integrates a vacuum interrupter (VI) and an ultrafast actuator that generates rapid contact separation. The operating principle relies on the vacuum arc voltage to commutate the current to a parallel semiconductor branch. As a result, the arc voltage directly relates to the overall breaker performance and therefore ultimately to the maximum interruption ratings. This fundamentally contrasts with alternating current (AC) switching applications, where low arc voltages are typically preferred to minimize the resulting arc power [4]. Therefore, modeling of the commutation process during opening operation is essential to develop cost-efficient and reliable HDCCBs. However, this requires in-depth knowledge of the arc voltage behavior during operation. In particular, one must know the arc voltage as a function of current and contact distance to predict the performance of an HDCCB under different fault current scenarios.

Kimblin [5] has reported a linear voltage against current characteristic at fixed contact distance and Miller [6] has reported a positive correlation between contact distance and arc voltage. However, the mutual influence of contact distance and current on the arc voltage has not yet been investigated and quantified.

In this study, we present the first model of the diffuse vacuum arc voltage as function of contact distance and current. First, we establish an experimental setup to determine the arc voltage under an independent variation of current and contact distance (Section 2). Based on the experimental results, we determine the model coefficients (Section 3) and analyze the model by comparing it to the original measurement data (Section 4). Moreover, we evaluate the limits of the model by discussing the formation of high-current anode modes.

2. Experimental setup

The experimental setup includes an industrially manufactured VI with Transverse Magnetic Field (TMF) contact system. The contacts are made of Cu75Cr25 and have a diameter of 45 mm. The VI is connected to a Thomson coil actuator prototype via a glass-fiber-reinforced plastic drive rod (Fig. 1). Upon start of the test, the Thomson coil actuator is energized by a current i_{TC} to open the VI, while simultaneously a rising test current i_{VI} is applied to the VI. Section 2.1 and 2.3 feature detailed descriptions of the Thomson coil actuator system, respectively the test current generation.

During the test, we measure the displacement of the actuator with a high-speed camera system as described in section 2.2. Additionally, we measure the VI current and the respective arc voltage using a transient recorder with a sampling rate of 100 MS/s.

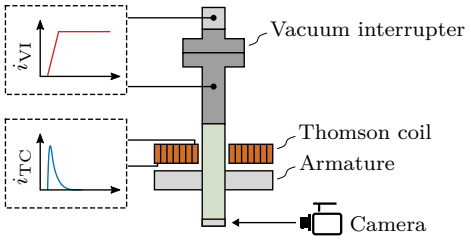

Figure 1. Representation of experimental setup.

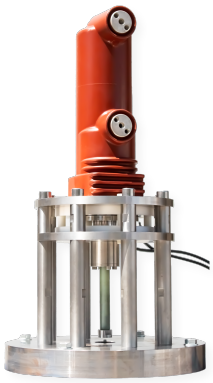

Figure 2. Thomson coil actuator connected to a vacuum interrupter.

2.1. Thomson coil actuator

The Thomson coil (TC) actuator is an electromagnetic repulsion-based linear actuator (Fig. 1 and 2). It features a fixed planar spiral coil and a movable armature disk. The disk is attached to a drive rod, which is connected to the movable contact of the VI. Applying an impulse current to the TC generates a magnetic field that induces eddy currents in the armature disk. This causes a repulsive Lorentz force that drives the linear displacement and ultimately opens the VI contacts. The Lorentz force likewise has an impulse shape, which means that after initial acceleration, the VI experiences almost linear motion which is only decelerated by friction, drag, and the mechanical load characteristics of the VI. In this prototype setup, the drive rod is positioned to contact a mechanical damper during opening phase, realizing a maximum contact distance of $d = 10\,\text{mm}$.

The impulse current circuit used to energize the TC uses a capacitor $C_{\text{TC}} = 828\,\mu\text{F}$ which is charged to $u_{\text{C}} = [300...900]\,V$, resulting in a stored electrical energy of 37 J–331 J (Fig. 3). By triggering the thyristor T an impulse current of up to 3373 A with a time to peak of 236 µs is generated. The diode D and resistance R_{D} limit the reverse voltage of the capacitor.

2.2. Displacement measurement

The displacement measurement is realized with a Phantom M310 high-speed camera to record the movement of the lower end of the drive rod (see Fig. 1). The camera records the movement of the drive rod with a frequency of 281 kS/s at a resolution of 640 pixels in

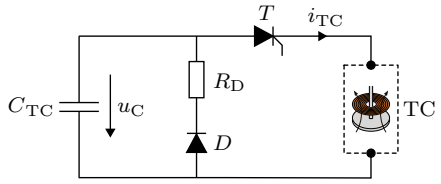

Figure 3. Impulse current circuit to energize the Thomson coil actuator.

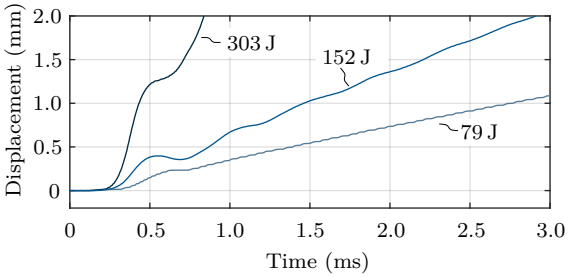

Figure 4. Measured actuator displacement.

the direction of movement. The short digital exposure time of 1 µs requires a 300 W LED light source to illuminate a round metal component, attached to the bottom end of the drive rod. In the camera footage, the illuminated metal component appears relatively bright compared to the less reflective drive rod. We utilize this sharp brightness transition to perform a motion tracking analysis.

To calibrate the digital motion to an absolute displacement value, we capture images at closed position ($d = 0\,\text{mm}$) and fully opened position ($d = 10\,\text{mm}$) before each measurement series. Using these images, we calculate the relationship between the pixel coordinates and the corresponding absolute position value. The camera is placed at a distance of approx. 20 cm to the drive rod and the resulting displacement resolution corresponds to 16 µm–18 µm per pixel.

Due to the impulse-shaped acceleration force of the Thomson coil actuator, the armature and drive rod experience material bending, causing measured displacement profiles to exhibit non-linear displacement profiles (Fig. 4). As a result, there can be a deviation between measured actuator displacement, which is measured at the bottom of the actuator, and contact distance, which is located at the top end of the arrangement. We performed a multiphysics simulation study using the model described in [7] to estimate that the maximum displacement difference can be in the range of 100 µm–200 µm, particularly during the initial acceleration phase.

2.3. Test current generation

The laboratory setup to generate the test current through the VI is based on a power electronic buck converter (Fig. 5). The capacitors $C_{\text{mod}} = 2\,\text{mF}$ are precharged to 150 V–1550 V to serve as a DC voltage source for the test circuit, while insulated Insulated-Gate Bipolar Transistors (IGBTs) paired with freewheeling diodes control the output current i_{VI} via the

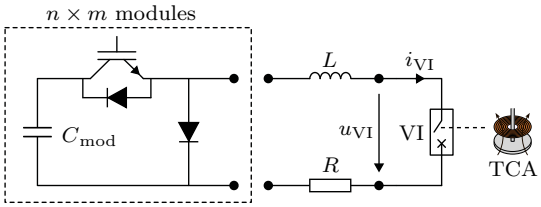

Figure 5. High-power test circuit for test current generation.

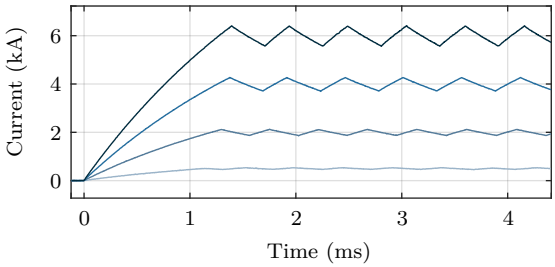

Figure 6. Measured rippled DC test current.

resistance $R = 200\,\mathrm{m\Omega}$ and inductance $L = 500\,\mu\mathrm{H}$. The test circuit is modularized with $n = 2$ modules in series and $m = 60$ modules in parallel to allow for an overall greater voltage and current rating. A detailed description of the laboratory setup and ratings, the operating principle, and the control implementation can be found in [8].

We employ the laboratory setup to generate rippled DC currents of $i_{\mathrm{VI}} = [500, 1000, ..., 6000]\,\mathrm{A}$ for a duration of 20 ms (Fig. 6).

3. Evaluation and modeling approach

In this study, we perform a full factorial combination of 12 different target VI current values and 7 different opening velocities. All tests are performed in a randomized order and a five-fold repetition, resulting in overall 420 experiments. We focus on modeling the diffuse arc voltage and exclude the microsecond-timeframe transition period from closed contacts to the diffuse arc mode. Therefore, we exclude all voltage signals lower 10 V to identify the time window of interest. The measurement data is downsampled to 281 kS/s, in order to match all signals to the sampling rate of the displacement measurement. In this time window of interest, we obtain a dataset of 1.76 million data tuples of voltage u_{VI}, current i_{VI} and displacement d from all experiments.

The obtained dataset is unbalanced, meaning that there are regions of current-displacement combinations where there are more data points compared to other regions. As a result, a fitted model becomes biased towards the majority region, leading to poor representation of the minority region. To address this, we perform data binning and discretize the current-displacement plane into discrete intervals, called bins. Original data values which fall into a given bin are aggregated to a single value, i.e., the mean of the samples belonging to that bin. The size of the bins should be chosen as small as possible, where ideally each bin contains at least one data point. In this study, we adopt bin intervals of 25 A and 50 µm to calculate the mean arc voltage value. Data binning has the tendency to give less weight to outlier measurement results, thus resulting in a usually better model fit compared to the original data set. We chose this method over a weighted fitting method, because it also reduces the size of the dataset to a reasonable level, whereas a weighted fitting method would require downsampling of the dataset.

The overall voltage drop of a diffuse vacuum arc depends largely on the current, contact distance, and the contact material, whereas a variation of the latter is excluded from this study. The voltage drop can be spatially and mathematically split in three components: 1) the cathode drop ϕ_{c}, which is independent of current and gap distance [5, 6]; 2) the plasma drop $\phi_{\mathrm{p}}(i, d)$, which increases with current and gap length [6]; and 3) the anode drop $\phi_{\mathrm{a}}(i)$ which increases with current but is independent of the gap distance [6]. Notably, Shkol'nik [9] has reported that the anode drop ϕ_{a} can become negative for currents below 900 A.

Considering the low resistance and inductance of the VI copper connections, we assume that the overall voltage drop over the entire VI is equal to the arc voltage, i.e., $u_{\mathrm{VI}} = u_{\mathrm{arc}}$. Furthermore, Heberlein [10] reports that the voltage drop of a diffuse vacuum arc can be considered independent of the instantaneous contact velocity and independent of the arc duration. Based on this, we propose the following modeling approach

$$\phi_{\mathrm{c}} = U_{\mathrm{c}} \tag{1}$$

$$\phi_{\mathrm{p}}(i, d) = i\, d\, \rho_{\mathrm{p}} \tag{2}$$

$$\phi_{\mathrm{a}}(i) = i\, R_{\mathrm{a}} - U_{\mathrm{a}} \tag{3}$$

where ρ_{p} is the length-dependent resistance of the plasma drop, and R_{a} is the resistance of the anode drop. The arc voltage is defined as the sum of the cathode, plasma and anode drop:

$$u_{\mathrm{arc}}(i, d) = \phi_{\mathrm{c}} + \phi_{\mathrm{p}}(i, d) + \phi_{\mathrm{a}}(i) \tag{4}$$

Since we measure the arc voltage as a whole and cannot distinguish between U_{c} and U_{a}, we define the constant voltage drop $U_0 = U_{\mathrm{c}} - U_{\mathrm{a}}$.

$$u_{\mathrm{arc}}(i, d) = U_0 + i\,(R_{\mathrm{a}} + d\,\rho_{\mathrm{p}}) \tag{5}$$

Other modeling functions have been considered but ultimately disregarded because of inferior model fit or introduction of higher complexity without improving the goodness of the model fit. This includes all polynomial terms of third order.

4. Results and Discussion

Table 1 shows the resulting regression coefficients of the model fit on the binned data. The model yields

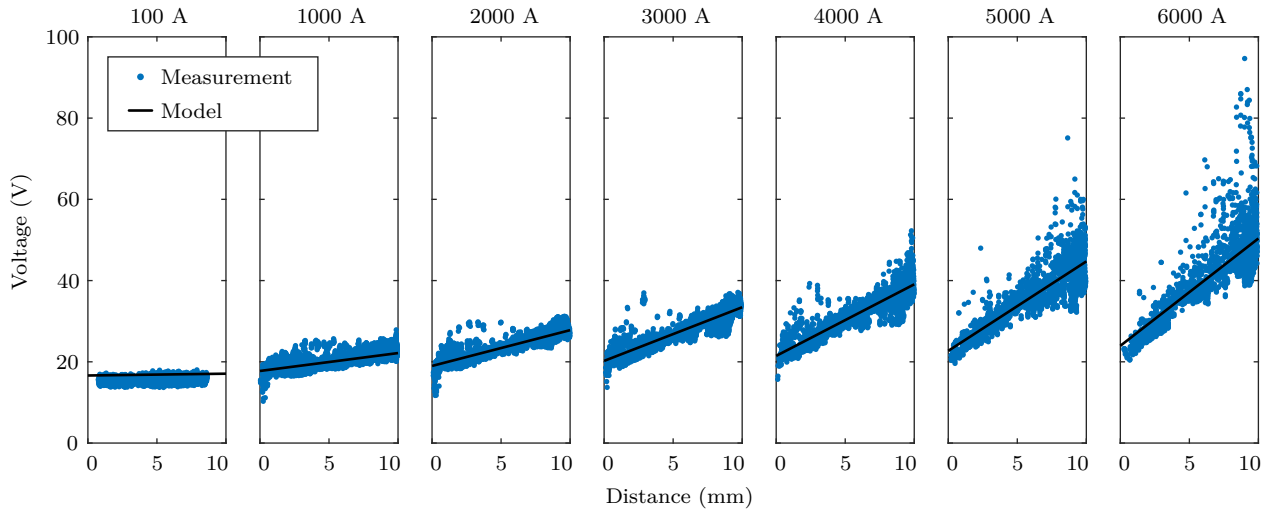

Figure 7. Measured and modeled arc voltage as a function of contact distance at seven discrete current levels.

Coefficient	Value
U_0	16.51 V
R_a	1.238 mΩ
ρ_p	0.4404 mΩ/mm

Table 1. Regression coefficients of diffuse vacuum arc voltage model

a coefficient of determination $R^2 = 97.8\,\%$ and root-mean-square error (RMSE) of 1.26 V, indicating a good level of accuracy in predicting the VI arc voltage across varying currents and contact distances. The model is tested against the original un-binned data set, resulting in $R^2 = 93.5\,\%$ and RMSE of 2.35 V. This improvement of the data fit performed on the binned data set is expected, as outlier measurements are averaged out in this method.

Figure 7 represents the original un-binned data compared to the model fit. For this illustration, data points in the current range of ± 10 A to each respective current level are displayed. From this representation, we can see that the general scatter in the measured voltage is around 5 V–10 V for current values of up to 4 kA. For larger currents, the voltage tends to be more scattered, particularly for comparatively high contact distances. This scatter tends to be a largely positive deviation compared to the model value. The mean value, however, still follows the model trend.

To analyze the cause of this scatter, we present two experiments featuring the same opening characteristic but different arc current (Fig. 8). The experiment featuring a DC current of 3 kA (red-colored curve in Fig. 8) has a nearly constant mean arc voltage of 35 V and comparatively low noise. It corresponds to the arc voltage model, with a slight tendency to overshoot the predicted value. On the other hand, in the experiment featuring a DC current of 6 kA (blue-colored curve in Fig. 8), we observe a sharp increase in noise

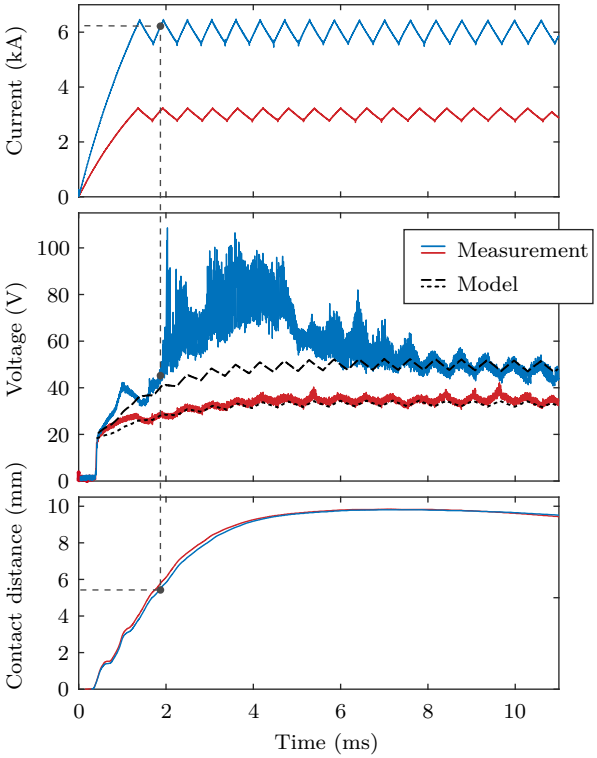

Figure 8. Time-dependent measured and modeled arc voltage of two experiments, featuring currents of 3 kA *(red-colored) and* 6 kA *(blue-colored) and similar opening characteristics.*

and mean arc voltage at $t = 1.9$ ms. At this point, the contacts reach a threshold distance of 5.5 mm. This observation is attributed to the contraction of the vacuum arc and the corresponding change of the anode mode. Miller [6] describes that there are at least seven different anode modes, of which particularly the Footpoint, the Anode Spot Type 1, and the Anode Spot Type 2 are associated with an increase in mean arc voltage. The appearance of these anode modes depends on many factors, including the contact distance; the anode contact diameter, material, and shape; the

current; and the magnetic field. From the measured data, we cannot make a conclusive determination of the anode mode that is transitioned towards—optical high-speed imaging of the vacuum arc would be necessary for that. However, Khakpour et al. [11] reported the appearance of a Footpoint mode featuring a similar test setup with DC current pulses of 3 kA at a contact distance of 8 mm. This anode mode is associated with a particularly high amount of noise, such as it was also observed in our test series. Interestingly, the voltage drops again at $t = 5$ ms and the noise gradually decreases, although current and contact distance are almost constant at this point. This observation corresponds to the findings of Miller [6] and Khakpour et al. [11], suggesting that the high-current anode mode formation is influenced by not only the threshold current and distance, but additionally the arcing time and transferred charge. At $t = 8$ ms, the mean arc voltage and noise has settled to a level that corresponds to the presented model and we assume that the arc is diffuse again.

5. Conclusions

We present a model that accurately determines the arc voltage of the diffuse vacuum arc as a function of the contact distance and current. This model enables future research to establish a correlation between the actuator of an arc commutation hybrid DC circuit breaker and the overall switching performance of such a breaker.

The model is based on three setup-specific coefficients, namely the constant voltage drop U_0, the resistance of the anode drop R_a, and the length-dependent resistance of the plasma drop ρ_p. In an experimental setup featuring an industrially manufactured vacuum interrupter, we exemplify a method to determine these model coefficients in great detail. For the given setup, the model is validated for a contact distance up to 10 mm and currents up to 5 kA. Based on our findings, the arc voltage in the diffuse arc mode is predictable, reproducible and robust to different actuator velocities and current rates-of-rise. We therefore suspect, one could achieve reliable determination of the introduced coefficients performing a low number of experiments. However, particular attention must be paid to the transition phase towards high-current arc modes. Beyond this, the voltage characteristic changes and the presented model is invalid. We confirm literature statements, suggesting that the formation of high-current anode modes likely depends not only on the contact distance and current, but additionally on the arc duration, respectively the transferred charge.

Acknowledgements

The authors would like to thank ABB for providing VIs to carry out the experimental investigations.

Funded by the Federal Ministry of Education and Research (BMBF, FKZ 03SF0595), Flexible Electrical Networks (FEN) Research Campus. The author is responsible for the content of this publication.

References

[1] J. Y. et al. and J. C6/B4.37. Tb 875 - medium voltage dc distribution systems. Technical report, CIGRE, 2022.

[2] C. H. et al. and W. A3.40. Tb 931 - technical requirements and field experiences with MV DC switching equipment. Technical report, CIGRE, 2024.

[3] J.-M. Meyer and A. Rufer. A DC hybrid circuit breaker with ultra-fast contact opening and integrated gate-commutated thyristors (igcts). *IEEE Transactions on Power Delivery*, 21, 2006. doi:10.1109/TPWRD.2006.870981.

[4] P. Slade. *The Vacuum Interrupter: Theory, Design, and Application*. CRC Press, 2nd ed. edition, 2020. ISBN 9780429298912. doi:10.1201/9780429298912.

[5] C. W. Kimblin. Anode voltage drop and node spot formation in dc vacuum arcs. *Journal of Applied Science*, 40, 1969. doi:10.1063/1.1657842.

[6] H. C. Miller. Anode modes in vacuum arcs: Update. *IEEE Transactions on Plasma Science*, 45(8), 2017. doi:10.1109/TPS.2017.2708695.

[7] P. Wienkamp, S. Kimpeler, F. Mingers, et al. Discretization study for 2D axisymmetric modeling of an ultrafast thomson coil actuator. In *2024 International Conference on Electrical Machines (ICEM)*, pages 1–7, Torino, Italy, 2024. doi:10.1109/ICEM60801.2024.10700458.

[8] N. Langenberg, S. Kimpeler, P. Wienkamp, et al. Innovative synthetic high-power test circuit for the investigation of MVDC circuit breakers – setup, functionality and application. In *VDE High Voltage Technology; 4. ETG-Symposium*, pages 1–6, Berlin, Germany, 2022.

[9] S. M. Shkolnik. Secondary plasma in the gap of high-current vacuum arc: origin and resulting effects. *IEEE Transactions on Plasma Science*, 31, 2003. doi:10.1109/TPS.2003.818442.

[10] J. V. R. Heberlein and J. G. Gorman. The high current metal vapor arc column between separating electrodes. *IEEE Transactions on Plasma Science*, 8, 1980. doi:10.1109/TPS.1980.4317328.

[11] A. K. et al. Impact of different vacuum interrupter properties on high-current anode phenomena. *IEEE Transactions on Plasma Science*, 44, 2016. doi:10.1109/TPS.2016.2625862.